Supporting information for:

Synthesis and Micellization of Bottlebrush Poloxamers

Joseph F. Hassler,[1] Nicholas J. Van Zee,[2] Adelyn, A. Crabtree,[1] Frank S. Bates,[1*] Benjamin, J. Hackel,[1*] Timothy P. Lodge[1,2*]

[1]Department of Chemical Engineering and Materials Science and [2]Department of Chemistry, University of Minnesota, Minneapolis, MN 55455

*Authors for correspondence: bates001@umn.edu, hackel@umn.edu, lodge@umn.edu

Materials:

All materials were used as received. The following materials were purchased from Sigma: propylene oxide, (>99.0%), butyl-magnesium chloride, potassium tert-butoxide, 18-crown-6 ether, palladium (10% on activated charcoal), 4-dimethylaminopyridine (>99%), N,N' diisopropylcarbodiimide (99%), exo-5-norbornene-2-carboxylic acid (97%), methyl ether poly(ethylene glycol) (M_n = 2000 g/mol), poly(ethylene oxide) (M_n = 20,000 g/mol), tetrahydrofuran (ACS reagent, 97%, stabilized with 250 ppm BHT), pyridine (>99%), ethyl vinyl ether (stabilized with 0.1% KOH, 99%), benzene (ACS reagent, 99%), sodium chloride (99.5%), potassium chloride (>99%), calcium chloride (anhydrous, 96%), magnesium chloride (97%), HEPES buffer (99.5%), tetrahydrofuran (anhydrous, 99.9%), second generation Grubbs Catalyst® M204, α-cyano-4-hydroxycinnamic acid, and sodium trifluoroacetic acid (98%). The following materials were purchased from Fisher Scientific: methanol (HPLC grade), diatomaceous earth (Celite), dichloromethane (ACS reagent, anhydrous, 99.8%), diethyl ether (anhydrous), and sodium sulfate (anhydrous). SiliaMetS DMT was purchased from Silicycle. Deuterated chloroform (99.8% d) was purchased from Cambridge Isotope Laboratories. Hydrogen gas was purchased from Airgas.

Methods:

Anionic polymerization of propylene oxide:

Synthesis of tert-butyl-poly(propylene oxide) (*t*-PPO-OH) was carried out through anionic polymerization. Details of the synthetic procedure can be found in previous publications.[1,2] Briefly, anionic polymerization was carried out in a water and air free environment under argon. Tetrahydrofuran was dried using an alumina column and used as the solvent. 18-crown-6-ether was used in a 2:1 molar ratio relative to potassium ions to reduce unwanted side reactions and increase conversion of PPO.[3,4] Propylene oxide was purified over butyl-magnesium chloride and added to the reactor. Potassium *t*-butoxide was added to initiate the reaction at 25 ºC and the reaction was stirred for 72 hr. The polymerization was terminated with acidic methanol. The resulting product was then subjected to repeated filtering and rotary evaporation followed by two hexane/ water liquid-liquid extractions in a separatory funnel were used to remove crown ether and salts from the product. The volume ratio of hexane: water was roughly 1:2 and the hexane phase was collected, dried over anhydrous sodium sulfate, and the solvent was removed with a rotary evaporator.

Hydrogenation of poly(propylene oxide):

An example hydrogenation protocol is as follows. Poly(propylene oxide) (PPO) polymer, faint yellow gel (1.19 g, 1.1 mmol) was put in a round bottom flask with palladium on carbon catalyst (0.27 g) at a 5:1 PPO: Pd/C by mass. The flask was gently rotated to coat the polymer with the catalyst. 10 mL of methanol was added, and the solution was stirred and bubbled with argon for 30 minutes. Hydrogen gas was collected using a balloon and syringe technique and added to the flask via a needle. A 25 gauge needle was used to displace argon with hydrogen for 1 minute. The reaction was stirred at room temperature overnight. The reaction effluent was diluted with methanol and filtered with Celite until the filtrate was clear. Solvent was evaporated using a rotary evaporator to yield a faint yellow gel (72% yield).

Esterification of PPO-OH:

An example esterification protocol is as follows. Hydrogenated PPO (0.83 g, 0.76 mmol) was dried using a vacuum line in a 20 mL scintillation vial. Then, 4-dimethylaminopyridine (DMAP) (0.019 g, 0.16 mmol) and exo-5-norbornene-2-carboxylic acid (0.16 g, 1.15 mmol) were added to the scintillation vial and dissolved in 4.5 mL anhydrous dichloromethane. Meanwhile, N,N' diisopropylcarbodiimide (DIC) (0.14 g, 1.14 mmol) was mixed with 1 mL of anhydrous dichloromethane. The DIC solution was then added dropwise to the reaction vial over 3 minutes while stirring. White precipitate formed within 30 minutes and the reaction was stirred at room temperature for 7 days. The reaction solution was filtered with a fine filter to remove the precipitate, and the effluent was diluted with hexanes and washed three times with a 0.1 M NaOH solution with addition of a small volume ~3 mL of saturated NaCl brine. The organic phase was dried over sodium sulfate, concentrated with a rotary evaporator to yield a faint yellow gel with crystals due to excess exo-5-norbornene-2-carboxylic acid. This mixture was then dried in a vacuum oven at 50 ℃ for 7 days where the crystals slowly sublimed to leave a yellow gel (90% yield).

Esterification of PEO-OH:

The same reaction protocol as for PPO esterification was performed, except the reaction was run for 48 hours. The reaction solution was filtered with a fine filter to remove the precipitate and dried on a rotary evaporator. The product was dissolved in tetrahydrofuran and the polymer was purified from the excess exo-5-norbornene-2-carboxylic acid by two precipitations in cold diethyl ether to yield a white powder (64% yield).

Grubbs catalyst preparation:

Second generation Grubbs catalyst (G2) [(H2IMes)(PCy3)Cl2Ru=CHPh] was purchased from Millipore sigma and converted to Grubbs third generation catalyst (G3) using an established procedure.[5] G2 (1.01 g, 1.2 mmol) was mixed with pyridine (3.0 g, 36 mmol) in a 50 mL round bottom flask and stirred in air for 10 minutes. An immediate color change from dark red to dark green was observed. 20 mL of pentane was layered on top and the flask was placed in a -20 ℃

freezer overnight. The product, green powder, was recovered via vacuum filtration and washed with excess pentane (98% yield).

Sequential Ring Opening Metathesis Polymerization (ROMP):

All ROMP reactions were done in a glovebox with an argon atmosphere ($[O_2] < 10$ ppm; $[H_2O] < 10$ ppm) with a monomer concentration of approximately 0.05 M in anhydrous dichloromethane and were stirred at room temperature for 10 minutes. Fresh G3 stock solution (dark green) and monomer stock solutions were prepared with precisely known molar concentrations. To initiate polymerization, a precise volume of G3 stock solution was added to the first monomer solution via a gas tight syringe such that the molar ratio of monomer to catalyst was equal to the target degree of polymerization. The solution quickly fades from dark green to rust brown upon initiation. The reaction was stirred for 10 minutes, then a minimal volume of the reaction was taken as an aliquot and quenched with a 1:1 (vol) mixture of ethyl vinyl ether: dichloromethane. The second monomer solution was added to the reaction vessel, again such that the molar ratio of monomer to catalyst was equal to the target degree of polymerization. The reaction was taken out of the glovebox and quenched by stirring with an equal volume of the ethyl vinyl ether: dichloromethane mixture for 10 minutes. G3 catalyst was removed by diluting the reaction with ~50 mL dichloromethane and stirring with several scoops of SiliaMetS-DMT (silicycle) for ~2 hours until the supernatant is clear. The silicycle with bound G3 was removed by filtering through a column of Celite. The effluent was dried with a rotary evaporator, dissolved in benzene and freeze dried to recover the polymer as a white powder. Typical yields are ~80%.

Polymer characterization:

^{1}H NMR: All NMR samples were prepared in deuterated chloroform at a sample concentration between 10 – 20 mg/mL. All spectra were collected using a Bruker Avance III HD-500 MHz spectrometer with a 5mm Prodigy TCl cryoprobe. Chemical shifts are reported in parts per million and were referenced to the residual chloroform peak at 7.26 ppm. ^{1}H NMR was used to quantify conversion, assess purity, and confirm polymer composition.

Size Exclusion Chromatography (SEC): All SEC samples were prepared in tetrahydrofuran at a concentration of 5 mg/mL and filtered with a 0.2 um PTFE filter. An instrument equipped with 2 phenogel columns and a Wyatt Dawn Heleos II multi-angle light scattering detector was used to obtain molecular weights and dispersities. The reported refractive index increment (dn/dc) of PEO and PPO in THF are 0.068 mL/g and 0.087 mL/g, respectively.[6] The dn/dc of all diblocks was taken as the weighted average of these components based on the targeted composition.[7]

MALDI-ToF: To prepare MALDI samples, a 30 mg/mL solution of α-cyano-4-hydroxycinnamic acid (CHCA), a 3 mg/mL polymer solution, and a 1 mg/mL sodium trifluoroacetic acid (NaTFA) solution, all in tetrahydrofuran were prepared. The CHCA and polymer solutions were mixed in a volume ratio of 2:1 and a drop of the NaTFA solution was added. An AB SCIEX TOF/TOF 5800 instrument was used in reflector mode. For every MALDI-ToF spectra collected, the laser power of the first shot was deliberately set too low to transfer the polymers into the gas phase. The laser power was then ramped in small steps until a clear spectrum was observed. Thus, all spectra reported were taken near the minimal laser power required, minimizing likelihood of sample degradation.

Micelle solution preparation:

Aqueous buffer was prepared according to an established recipe.[8] The buffer solution is 140 mM NaCl, 5 mM KCl, 2.5 mM $CaCl_2$, 2 mM $MgCl_2$, and 10 mM HEPES, which was prepared in milliQ water (18 Ω) and pH adjusted to pH = 7.2 with NaOH. Micelle stock solutions were prepared via direct dissolution, and a vortexer was used to facilitate dissolution. To ensure complete dissolution, solutions were held at 4 ℃ for 1 hour. Each series of micelle solutions was then prepared via serial dilution and were annealed at 37 ℃ overnight prior to measurements.

Dynamic Light Scattering (DLS):

DLS experiments were performed with a Brookhaven BI-200SM instrument equipped with a 637 nm laser and an adjustable goniometer. All measurements were done at 37 ℃ in a refractive index matching bath. All solutions were filtered with a 0.2 um GHP filter into clean glass test tubes (200 mm x 7 mm with 5 mm inner diameter) and sealed with parafilm. All excess scattering

intensity measurements were performed at a detector angle of 90°, a laser power of 5 mW, and an aperture setting of 400 nm. Intensity autocorrelation functions, $g_2(t)$ were recorded for a minimum of 5 minutes.

The Siegert relation was applied to convert $g_2(t)$ to the electric field autocorrelation function, $g_1(t)$. $g_1(t)$ was then fit to a second-order cumulant model (Eq. S1) and a two-exponential model (Eq. S2) and the residuals were compared (Figs. S11-S13).

$$g_1(t)=\exp(-2\Gamma t+k_2t^2) \quad \text{(S.1)}$$

$$g_1(t)=f_1\exp(-2\Gamma_1 t)+f_2\exp(-2\Gamma_2 t) \quad \text{(S.2)}$$

The mutual diffusion coefficient, D_m, of a species can be obtained by dividing the decay coefficient (Γ in the equations above) by the scattering vector q given by $q = (4\pi n/\lambda)\sin(\theta/2)$ where n is the refractive index of the medium, λ is the wavelength of the laser, and θ is the angle of detection. For dilute solutions, the mutual diffusion coefficient (D_m) and the tracer diffusion coefficient (D_t) are roughly the same. D_t can then be related to the hydrodynamic radius via the Stokes-Einstein equation.

Cryo-TEM:

For sample vitrification, 200 mesh lacey carbon copper grids (Ted Pella) were exposed to glow discharge to increase their surface energy. They were then transferred to an environmentally controlled chamber (FEI Vitrobot Mark III), which was held at 25 °C and 100% humidity. 5 μL of a 10 mg/mL polymer solution was then deposited onto the grid and blotted for 7 s. It was then allowed to anneal for 1 s before being plunged into a vat of liquid ethane. The samples were stored in liquid nitrogen prior to imaging. Imaging was performed using an FEI Technai Spirit Bio-Twin TEM at an accelerating voltage of 120 keV. Samples were kept at -176 ± 1 °C during imaging. Images were captured using a magnification of 40000× and an under-focus of approximately -20. Image analysis was performed using ImageJ software, and the built-in enhance local contrast filter was applied to all images. A minimum of 10 objects were measured in each image, and at least two grid locations were included in every analysis.

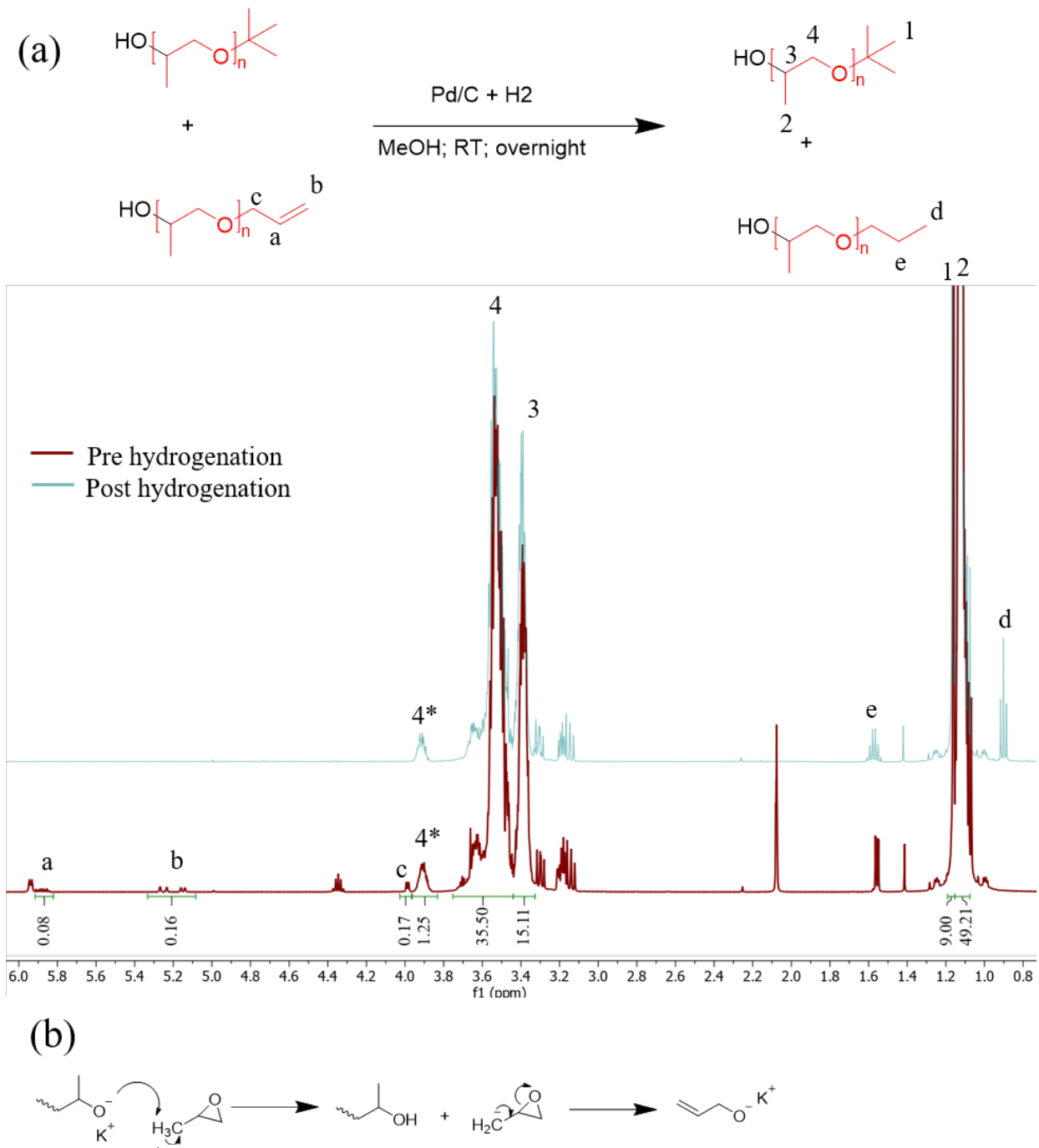

Figure S1. (a) ^{1}H NMR analysis of the pre-hydrogenation and post-hydrogenation PPO polymer. Note the disappearance of peaks a, b, and c from the alekene α-endgroup. (b) Chain transfer to monomer mechanism which leads to an alkene initiator species and results in the alkene α-endgroup impurity during anionic polymerization.[3]

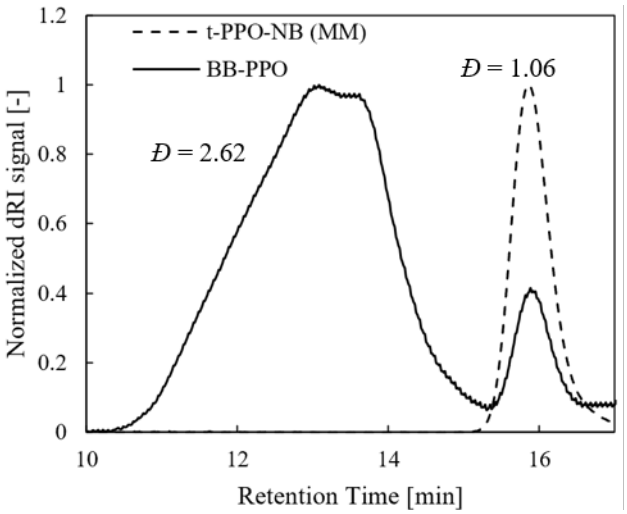

Figure S2. Effect of the alkene α-endgroup impurity on the ROMP reaction. SEC with refractive index detection of a *t*-PPO-NB macromonomer and the bottlebrush polymer resulting from ROMP when the macromonomer was not hydrogenated. The dispersity is large and there is unreacted monomer, indicating that control over the polymerization is lost.

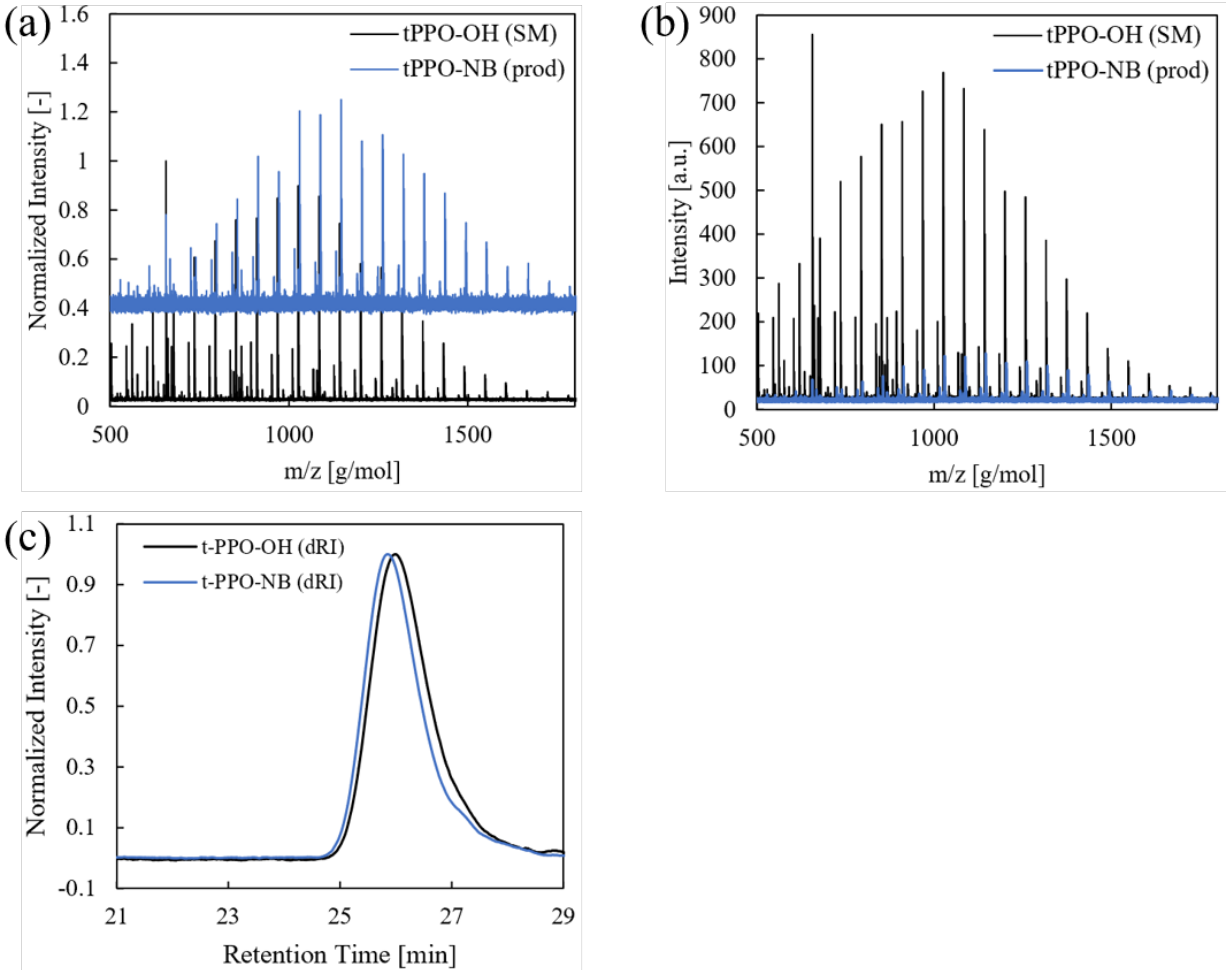

Figure S3. (a) Full, normalized MALDI spectra of the *t*-PPO$_{15}$-R materials shown in Fig. 2. Black is the starting material prior to hydrogenation and blue is the product of the esterification step (vertically shifted). (b) Comparison of the absolute intensity of the MALDI spectra as a function of the ω-end group. The alcohol (black) and NB (blue) appear to impact the ability of the polymer to ionize and/or fly, as the preparation protocol and laser intensity were identical. (c) Comparison of the SEC(dRI) traces of the *t*-PPO-OH prior to hydrogenation and the functionalized *t*-PPO-NB macromonomer post hydrogenation and esterification. The overlap of these chromatograms suggests that these reactions did not cause chain coupling or degradation.

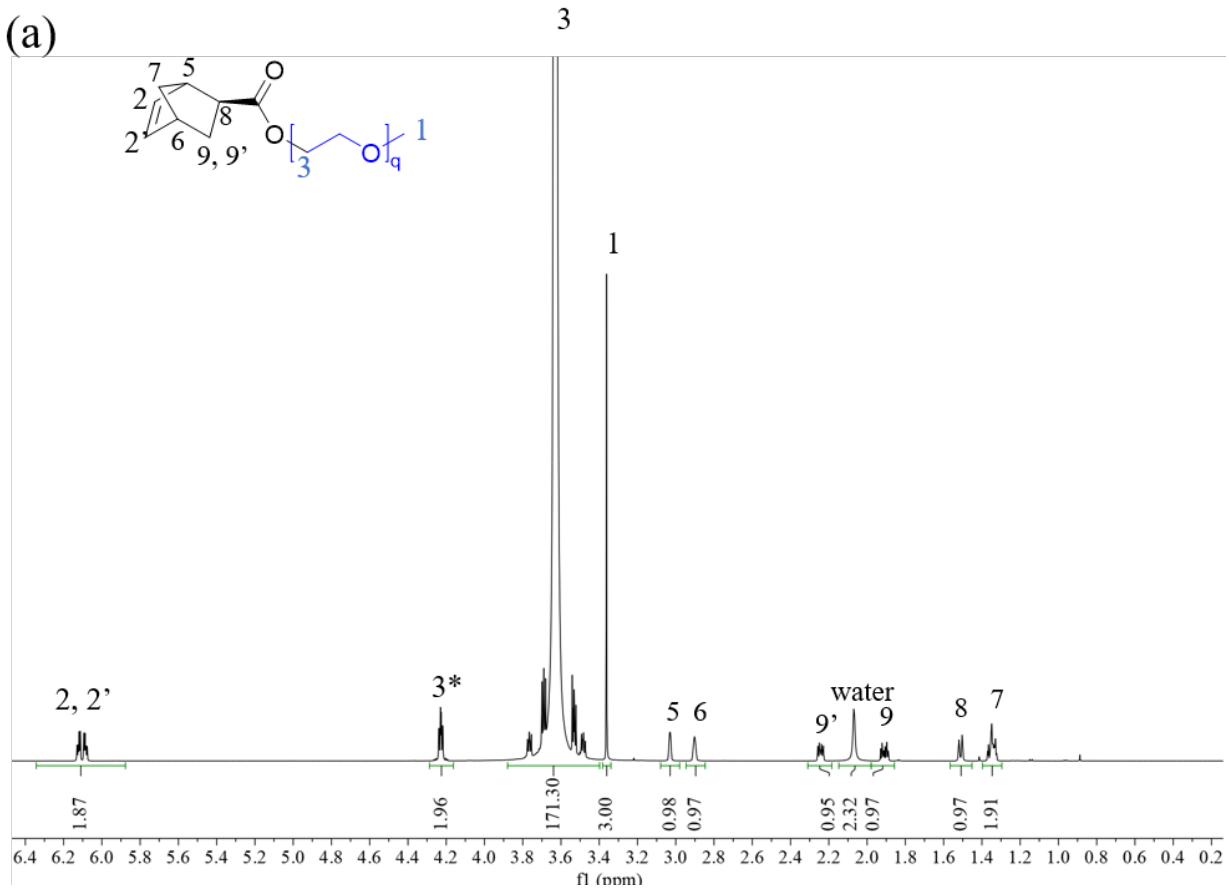
(a)
3
7
5
2
2'
8
6
9, 9'
O
O
3
O
q
1
1
2, 2'
3*
5
6
water
9'
9
8
7
1.87
1.96
171.30
3.00
0.98
0.97
0.95
2.32
0.97
0.97
1.91
6.4 6.2 6.0 5.8 5.6 5.4 5.2 5.0 4.8 4.6 4.4 4.2 4.0 3.8 3.6 3.4 3.2 3.0 2.8 2.6 2.4 2.2 2.0 1.8 1.6 1.4 1.2 1.0 0.8 0.6 0.4 0.2
f1 (ppm)

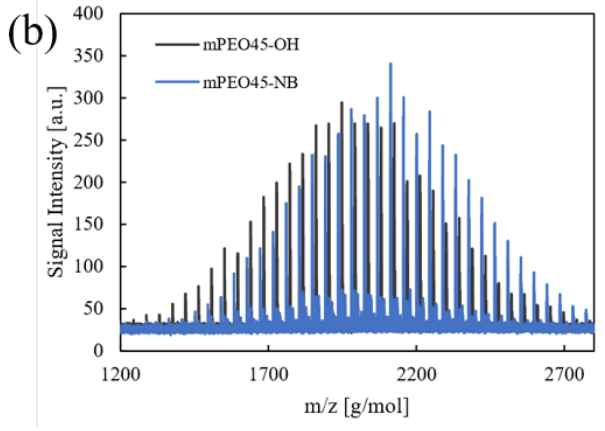
(b)
mPEO45-OH
mPEO45-NB
Signal Intensity [a.u.]
400
350
300
250
200
150
100
50
0
1200
1700
2200
2700
m/z [g/mol]

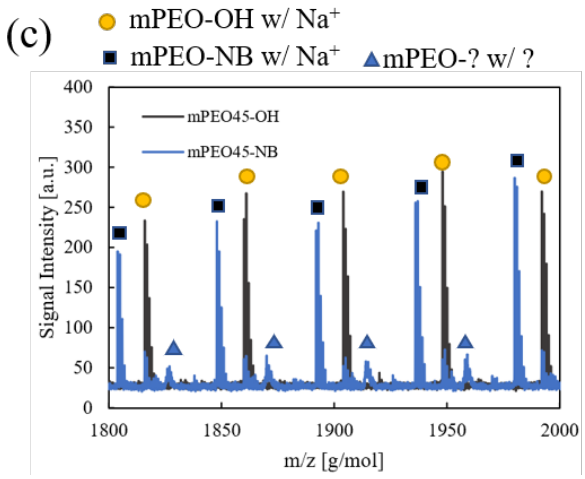

Figure S4: characterization of PEO-NB macromonomer. (a) ^{1}H NMR spectrum of the purified methyl terminated PEO2k-NB macromonomer. The peak shape of peak 2, 2' indicates that all excess norbornene small molecule was removed via the precipitations. The ratio of the norbornene end group to the methyl end group suggests the conversion of alcohol to norbornene was 94%. (b) MALDI of the starting material (mPEO-OH: M_n = 1970 g/mol, $Đ$ = 1.04) and the product (mPEO-NB - M_n = 2049 g/mol, $Đ$ = 1.03). The shift to higher molecular weight suggests successful addition of a norbornene end group; however, the shift in Mn is less than the molecular weight difference between norbornene and alcohol because a fraction of the chains (~6%) do not react and the ionizability of these two populations are not the same. Extending the mass range recorded in the MALDI to 5500 g/mol indicated that no chain coupling occurred (data not shown). (c) Zoom in on the MALDI spectra from 1800-2000 g/mol. Gold circle corresponds to unreacted alcohol endgroups (mPEO-OH), black square corresponds to the desired mPEO-NB, and blue triangles is a methyl terminated PEO with an undetermined ω chain end that does not interfere with ROMP and is a small fraction of the sample.

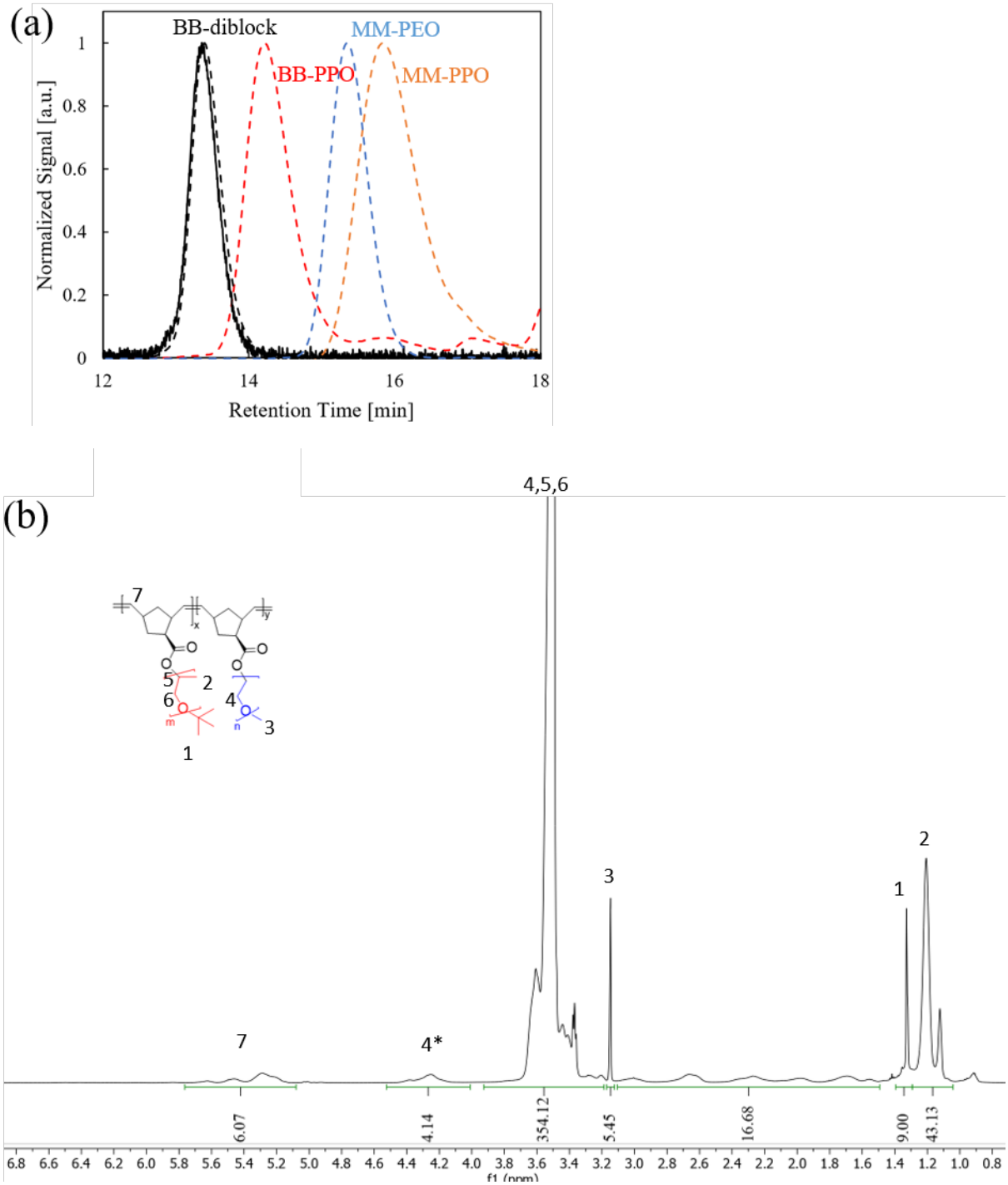

Figure S5: Characterization of BB-E$_{45,10}$-*b*-BB-P$_{15,5}$. (a) SEC chromatograms for both monomers, the BB-PPO block aliquot and the BB-PEO-b-BB-PPO diblock with the refractive index (dashed) and light scattering (solid) traces shown. From Zimm analysis M_n = 6,000 g/mol and $Đ$ = 1.31 for the BB-PPO aliquot and M_n = 26,200 g/mol and $Đ$ = 1.07 for the diblock. The resulting composition is 72 wt% PEO. (b) ^{1}H NMR spectrum for the diblock. The ratio of the methyl graft chain ends (3) to the backbone alkene peaks (7) gives an estimate of the composition of the polymer of 77 wt% PEO, confirming the SEC result. The absence of the monomeric NB peak at 6.0-6.2 ppm indicates full conversion of macromonomer.

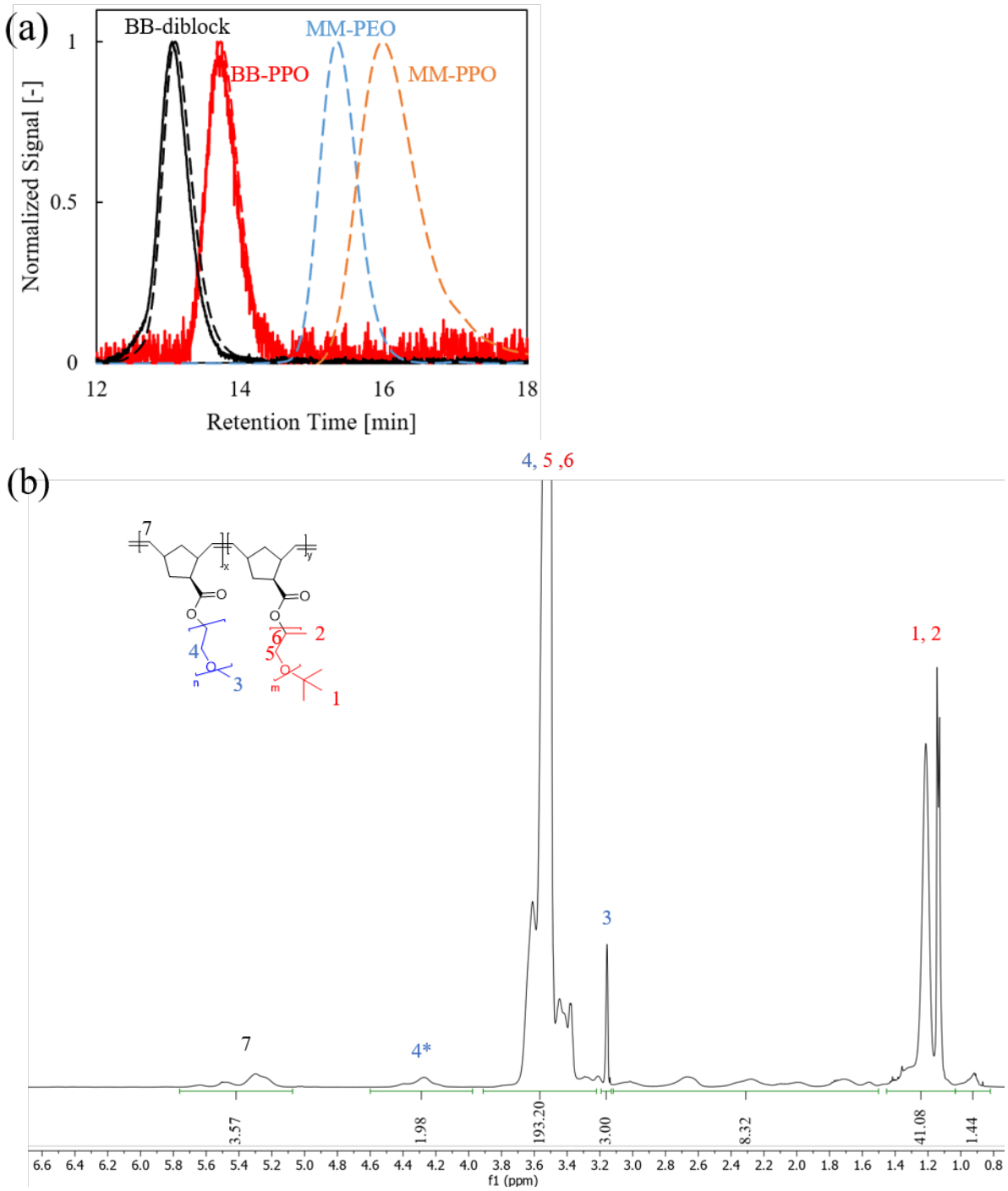

Figure S6: Characterization of BB-E$_{45,20}$-*b*-BB-P$_{15,10}$. (a) SEC chromatograms for both monomers, the BB-PPO block aliquot and the BB-PEO-b-BB-PPO diblock with the refractive index (dashed) and light scattering (solid) traces shown. From Zimm analysis M_n = 11,600 g/mol and $Đ$ = 1.20 for the BB-PPO aliquot and M_n = 55,300 g/mol and $Đ$ = 1.10 for the diblock. The resulting composition is 74 wt% PEO. (b) ^{1}H NMR spectrum for the diblock. The ratio of the methyl graft chain ends (3) to the backbone alkene peaks (7) gives an estimate of the composition of the polymer of 72 wt% PEO, confirming the SEC result. The absence of the monomeric NB peak at 6.0-6.2 ppm indicates full conversion of macromonomer.

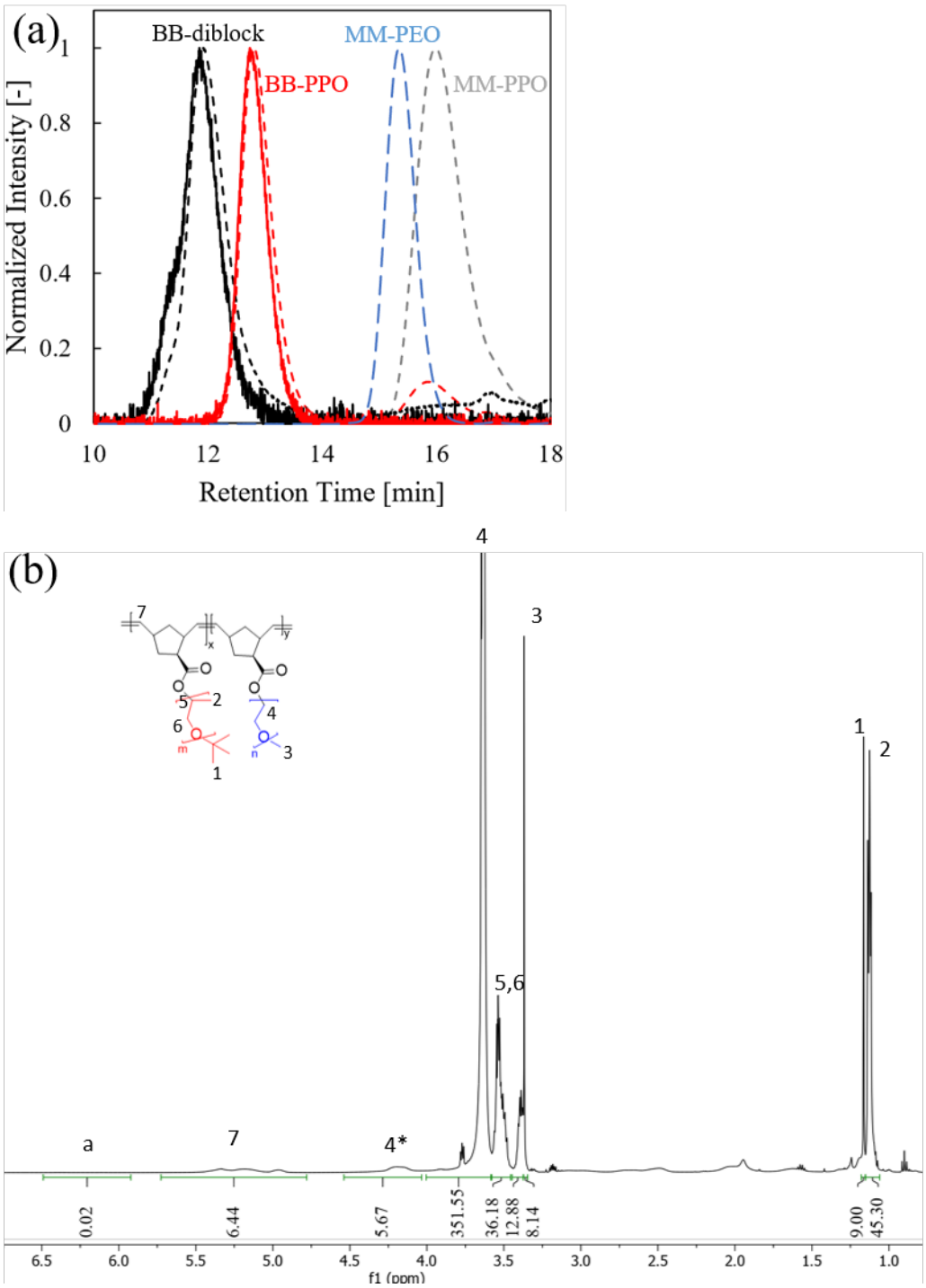

Figure S7: Characterization of BB-E$_{45,160}$-*b*-BB-P$_{15,43}$. (a) SEC chromatograms for both monomers, the BB-PPO block aliquot and the BB-PEO-b-BB-PPO diblock with the refractive index (dashed) and light scattering (solid) traces shown. From Zimm analysis M_n = 46,800 g/mol and $Đ$ = 1.09 for the BB-PPO aliquot and M_n = 394,000 g/mol and $Đ$ = 1.15 for the diblock. The resulting composition is 82 wt% PEO. (b) ^{1}H NMR spectrum for the diblock. The ratio of the methyl graft chain ends (3) to the backbone alkene peaks (7) gives an estimate of the composition of the polymer of 80 wt% PEO, confirming the SEC result. The small monomeric NB peak at 6.0-6.2 ppm (a) indicates ~99% conversion of macromonomer.

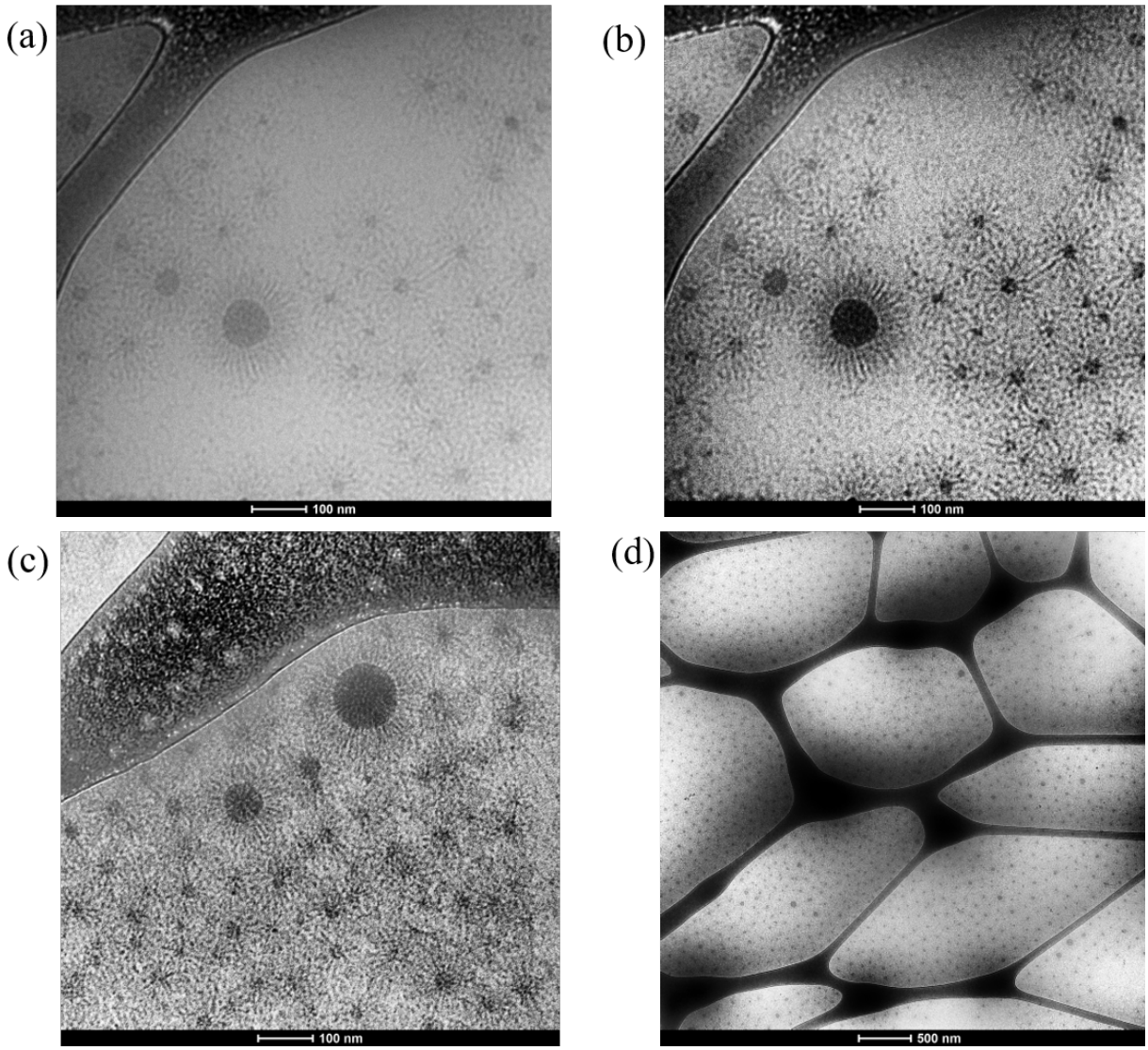

Figure S8: additional cryo-TEM micrographs of micelles of BB-$E_{45,160}$-*b*-BB-$P_{15,43}$. (a) Magnification of 40,000x and the same spot on the grid as Figure 4b in the main text but with reduced exposure time. No beam damage is observable on the grid. (b) Same image as in panel (a) after the enhance local contrast filter has been applied. (c) 40,000x magnification on an additional spot on the grid. (d) 8,000x magnification of an additional spot on the grid.

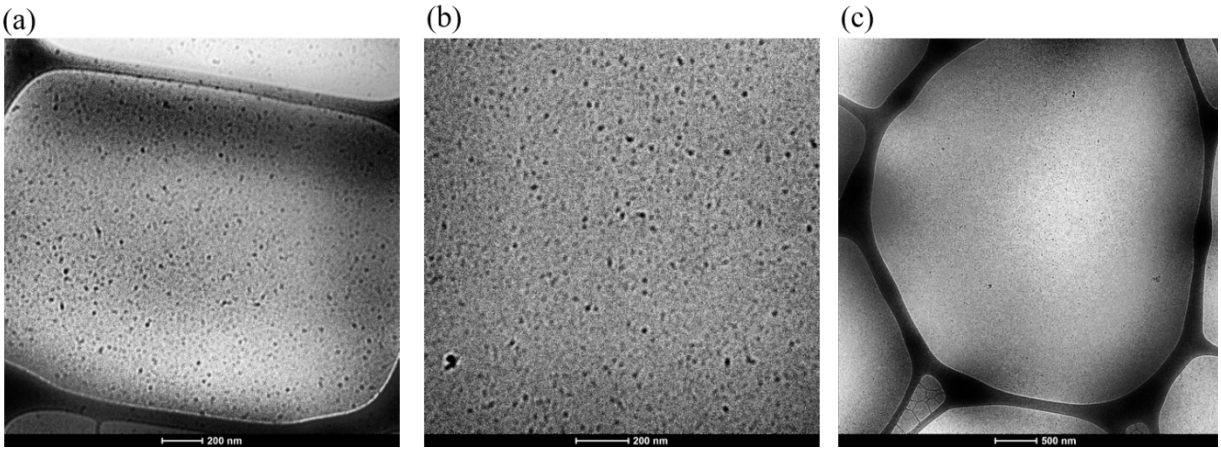

Figure S9: cryo-TEM micrographs of micelles of BB-$E_{45,10}$-*b*-BB-$P_{15,5}$. (a) Magnification of 20,000x and the same spot on the grid as Figure 4b in the main text but with reduced exposure time. No beam damage is observable on the grid. (b) 20,000x magnification on an additional spot on the grid. (c) 8,000x magnification of an additional spot on the grid.

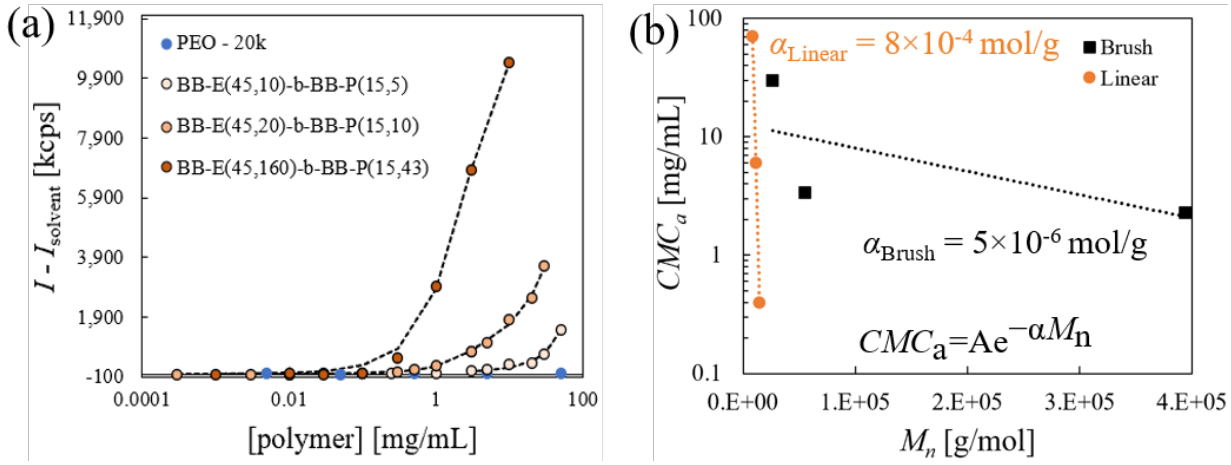

Figure S10: Closed association modelling as an alternative method to assess CMC_a. (a) Excess scattering intensity of each polymer fit to the closed association model described below. (b) The relationship between M_n and CMC_a where the CMC_a has been defined based on the model results. The same trend and scaling exponent as shown in Figure 4c are apparent.

The purpose of this analysis is to apply a model to define the apparent critical micellization concentration CMC_a; thus, removing all human decision making in the cut-off between the free-chain and micelle regimes. The details of the model used are shown below.

From light scattering theory, the excess scattering intensity depends on the product of the size and number of scatterers. Thus, for a mixture of unimers and micelles, the excess scattering intensity is given by Equation S3 below.[9]

$$I_{ex}=A[\text{unimers}]+B[\text{micelles}] \quad \text{(S3)}$$

The closed association model asserts that for a solution at a concentration above the CMC_a, an equilibrium between unimers at a concentration equal to the CMC_a and micelles of a constant number of chains, N_{agg}. This is expressed by the expressions shown below

$$N_{agg}\ \text{unimers} \leftrightarrow \text{micelle} \quad \text{(S4)}$$

$$[\text{unimers}]=\begin{cases}[\text{polymer}], & [\text{polymer}] < CMC_a \\ CMC_a, & [\text{polymer}] \geq CMC_a\end{cases} \quad \text{(S5)}$$

From a mol balance on the system, we can express the concentration of micelles as a function of the total concentration of polymer, chosen by the experimenter, the concentration of unimers and the aggregation number:

$$[\text{micelles}]=\frac{[\text{polymer}]-[\text{unimer}]}{N_{agg}} \quad \text{(S6)}$$

Now, we can express equation S3 using with a conditional expressing using only experimental quantities, [polymer], and model parameters: CMC_a, N_{agg}, A, and B:

$$I_{ex}=\begin{cases} A[polymer],\ [polymer]<CMC_a \\ A\times CMC_a + B\times \frac{[polymer]\text{-}CMC_a}{N_{agg}},\ [polymer]\geq CMC_a \end{cases} \quad (S7)$$

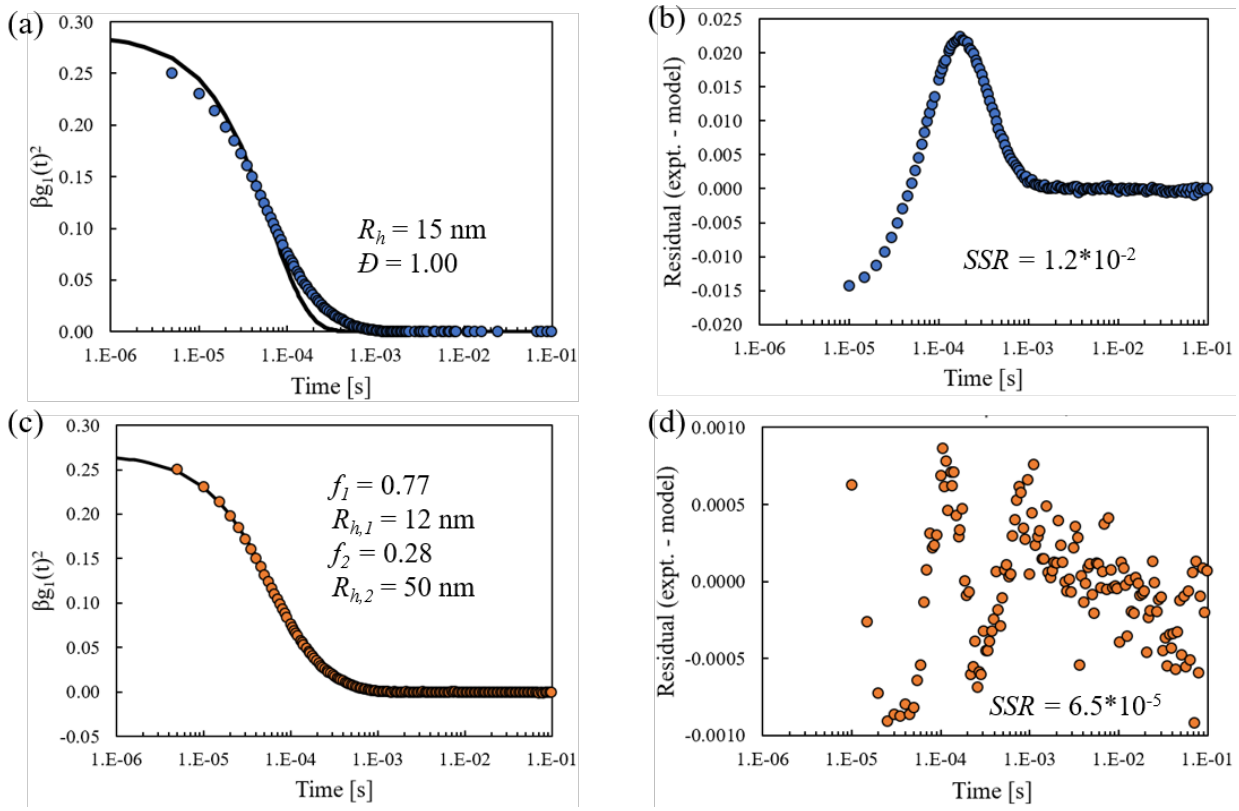

Figure S11: DLS correlation function fitting for micelle solution of BB-E$_{45,10}$-*b*-BB-P$_{15,5}$ at 10 mg/mL and 37 °C. (a) Fitting of the electric field autocorrelation function to the second cumulant model (Eq. S1). (b) Residuals between the data and the fit for the second cumulant model. (c) Fitting of the electric field autocorrelation function to a biexponential model (Eq. S2). (d) Residuals between the data and the fit for the biexponential model.

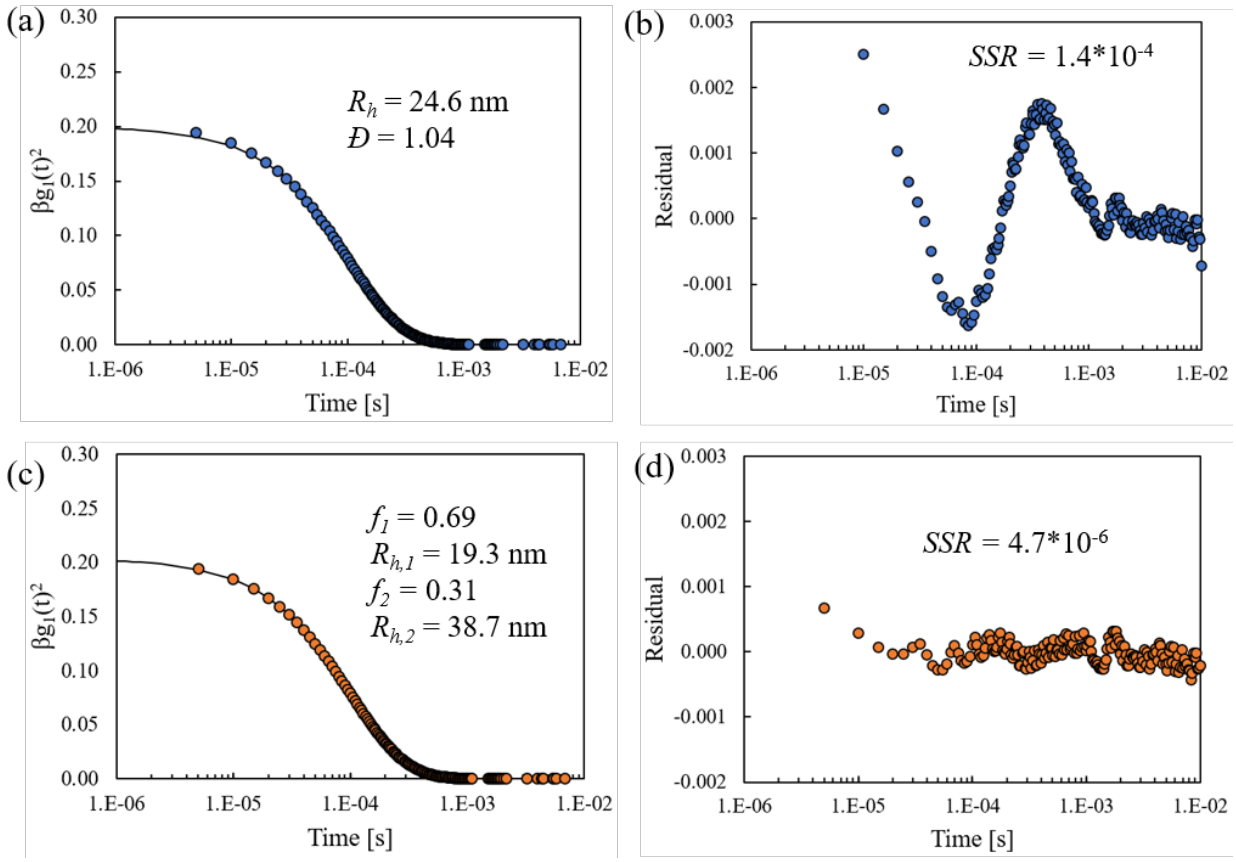

Figure S12: DLS correlation function fitting for micelle solution of BB-$E_{45,20}$-*b*-BB-$P_{15,10}$ at 10 mg/mL and 37 °C. (a) Fitting of the electric field autocorrelation function to the second cumulant model (Eq. S1). (b) Residuals between the data and the fit for the second cumulant model. (c) Fitting of the electric field autocorrelation function to a biexponential model (Eq. S2). (d) Residuals between the data and the fit for the biexponential model.

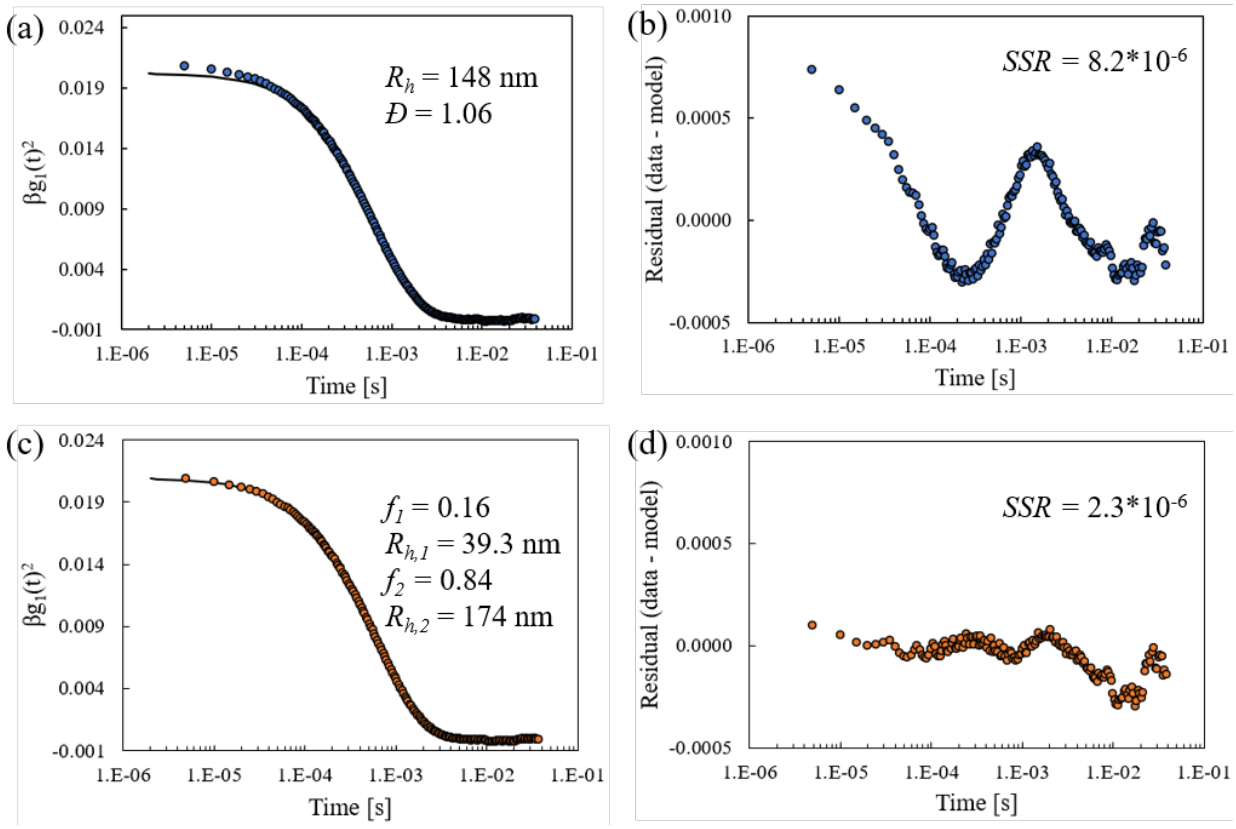

Figure S13: DLS correlation function fitting for micelle solution of BB-E$_{45,160}$-*b*-BB-P$_{15,43}$ at 10 mg/mL and 37 °C. (a) Fitting of the electric field autocorrelation function to the second cumulant model (Eq. S1). (b) Residuals between the data and the fit for the second cumulant model. (c) Fitting of the electric field autocorrelation function to a biexponential model (Eq. S2). (d) Residuals between the data and the fit for the biexponential model.

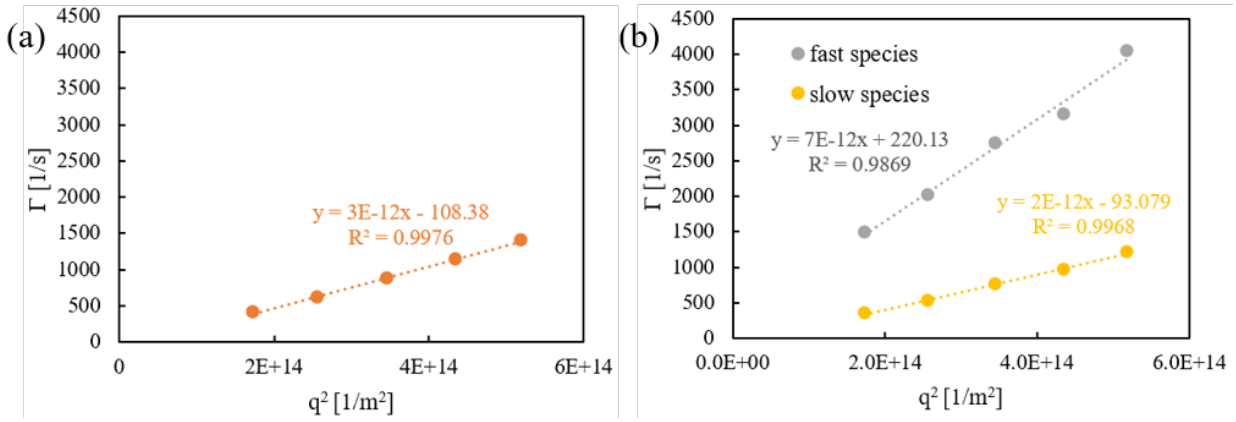

Figure S14: Multi-angle DLS data for micelle solution of BB-E$_{45,160}$-*b*-BB-P$_{15,43}$ at 3 mg/mL and 37 °C. (a) Γ found from the second cumulant model (Eq. S1). The slope gives a diffusion coefficient of 3×10^{-12} m^2/s. Based on the Stokes-Einstein equation this corresponds to a hydrodynamic radius of R_h = 110 nm. The near zero intercept and the high R^2 value suggests the relaxation process is diffusive. (b) Γ_1 and Γ_2 found from the biexponential model (Eq. S2). Similarly to the description of part (a), the slopes in this figure correspond to species with hydrodynamic radii of $R_{h,1}$ = 47 nm and $R_{h,2}$ = 160 nm. The linearity and high R^2 values suggest that both relaxation processes are diffusive.

Table S1: summary of biexponential model fitting of DLS data for 10 mg/mL micelle solutions.

Polymer	M_n [g/mol]	$Đ$	wt% PEO	wt% NB	$R_{h,\,small}$ [nm]	$R_{h,\,large}$ [nm]	f_{large}
BB-$E_{45,10}$-*b*-BB-$P_{15,5}$	26200	1.07	72	8	12 ± 0.2[a]	53 ± 2[a]	0.32 ± 0.04[a]
BB-$E_{45,20}$-*b*-BB-$P_{15,10}$	55000	1.10	74	8	19	39	0.31
BB-$E_{45,160}$-*b*-BB-$P_{15,43}$	394000	1.15	80	7	39	170	0.84

[a] Error reported from three independent replicates.

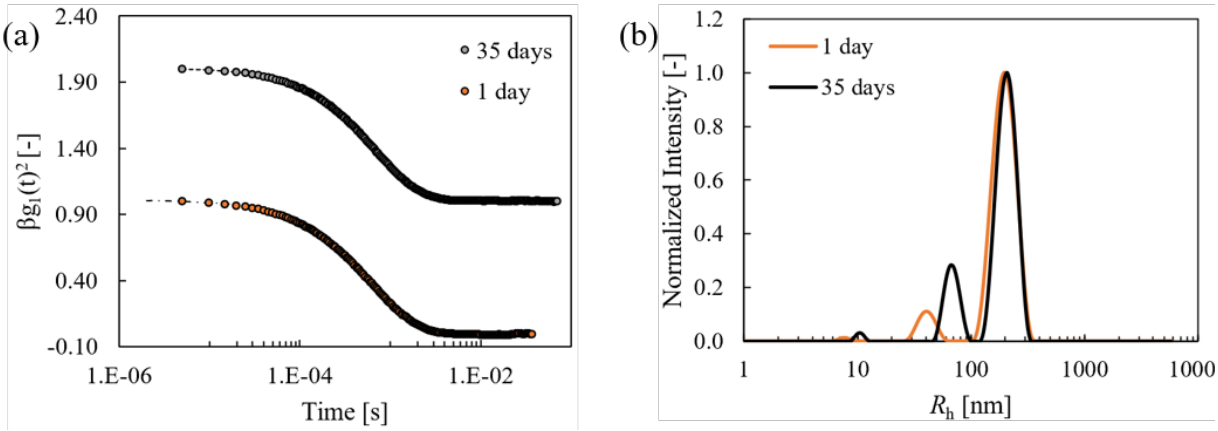

Figure S15: stability of micelle size distribution over a 35 day anneal at 37 °C. After the day 1 measurement was performed, the sample was recovered and placed in a sealed scintillation vial on a hotplate for 35 days. (a) Correlation function and analysis of a micellar solution of BB-$E_{45,160}$-*b*-BB-$P_{15,43}$ at 10 mg/mL. The data is fit to the biexponential model and the data is summarized in Table S2, below. (b) REPES analysis of the same correlation functions shown in panel (a). Both size distributions show a bimodal population and the sizes of both populations are within error.

Table S2: effect of anneal time on biexponential model fitting parameters

Time of anneal	$R_{h,\,small}$ [nm][c]	$R_{h,\,large}$ [nm][c]	f_{large}
1 day	39	170	0.84
35 days	64	200	0.89

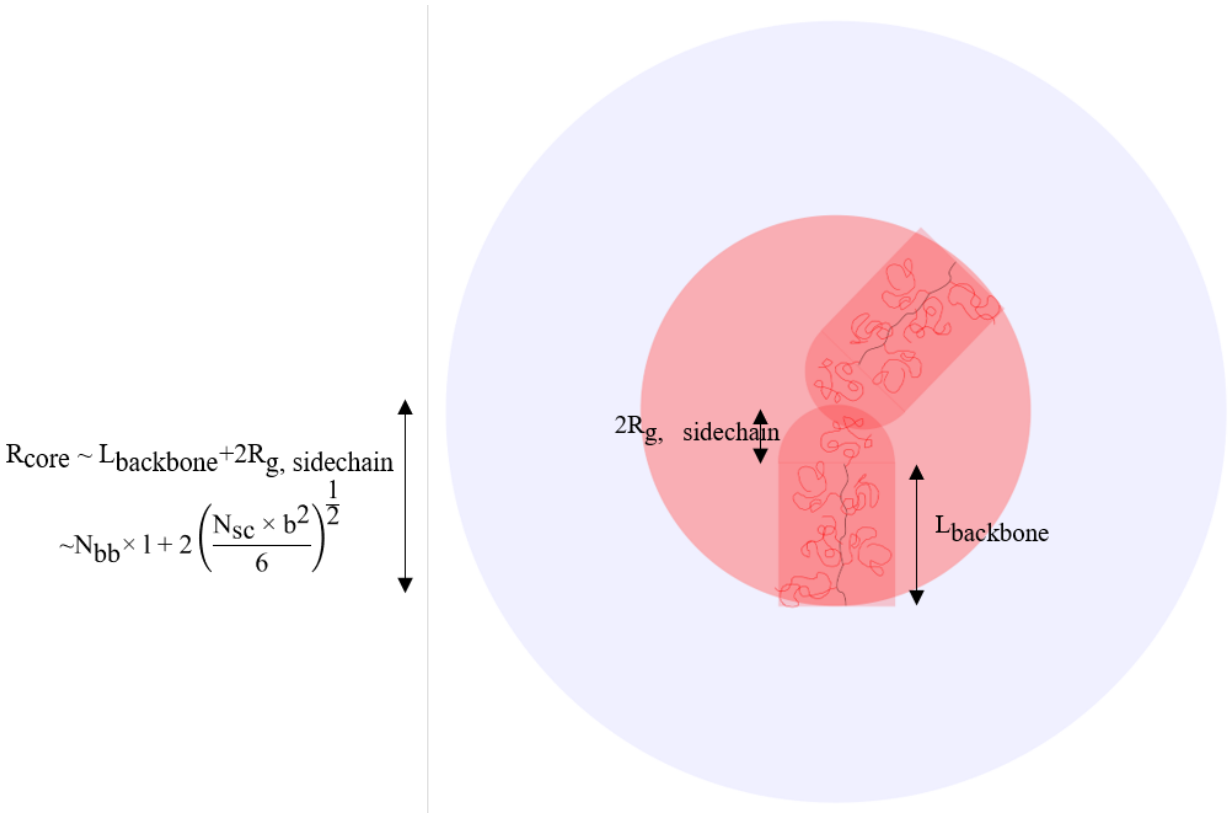

Figure S16: model of micelle core dimensions. This sketch illustrates the model used to estimate the micelle core dimensions from the polymer backbone and side chain degrees of polymerization. The model assumes that the backbone is a rigid rod, the side chains are gaussian coils, and there is no chain overlap; thus, this model serves as an upper bound of micelle core dimensions. Note this is a two-dimensional projection, so the side chain crowding is exaggerated because in three dimensions, side chains will have more space to avoid one another.

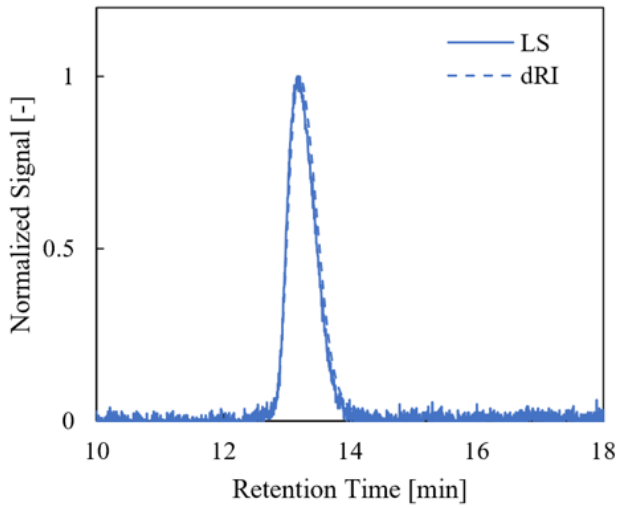

Figure S17: SEC characterization of linear PEO20k. The refractive index (dashed) and light scattering (solid) traces overlap and show a single peak with narrow distribution. From Zimm analysis of the light scattering data, the M_n = 20,000 g/mol and $Đ$ = 1.10.

References

(1) Ndoni, S.; Papadakis, C. M.; Bates, F. S.; Almdal, K. Laboratory-Scale Setup for Anionic Polymerization under Inert Atmosphere. *Rev. Sci. Instrum.* **1995**, *66* (2), 1090–1095.

(2) Hillmyer, M. A.; Bates, F. S. Synthesis and Characterization of Model Polyalkane - Poly (Ethylene Oxide) Block Copolymers. **1996**, *9297* (96), 6994–7002.

(3) Ding, J.; Heatley, F.; Price, C.; Booth, C. Use of Crown Ether in the Anionic Polymerization of Propylene Oxide-2. Molecular Weight and Molecular Weight Distribution. *Eur. Polym. J.* **1991**, *27* (9), 895–899.

(4) Allgaier, J.; Willbold, S.; Taihyun, C. Synthesis of Hydrophobic Poly(Alkylene Oxide)s and Amphiphilic Poly(Alkylene Oxide) Block Copolymers. *Macromolecules* **2007**, *40* (3), 518–525.

(5) Love, J. A.; Morgan, J. P.; Trnka, T. M.; Grubbs, R. H. A Practical and Highly Active Ruthenium-Based Catalyst That Effects the Cross Metathesis of Acrylonitrile. *Angew. Chemie - Int. Ed.* **2002**, *41* (21), 4035–4037.

(6) Zhang, W.; Haman, K. J.; Metzger, J. M.; Hackel, B. J.; Bates, F. S.; Lodge, T. P. Quantifying Binding of Ethylene Oxide-Propylene Oxide Block Copolymers with Lipid Bilayers. *Langmuir* **2017**, *33* (44), 12624–12634.

(7) Medrano, R.; Laguna, M. T. R.; Saiz, E.; Tarazona, M. P. Analysis of Copolymers of Styrene and Methyl Methacrylate Using Size Exclusion Chromatography with Multiple Detection. *Phys. Chem. Chem. Phys.* **2003**, *5* (1), 151–157.

(8) Kim, M.; Haman, K. J.; Houang, E. M.; Zhang, W.; Yannopoulos, D.; Metzger, J. M.; Bates, F. S.; Hackel, B. J. PEO-PPO Diblock Copolymers Protect Myoblasts from Hypo-Osmotic Stress in Vitro Dependent on Copolymer Size, Composition, and Architecture. *Biomacromolecules* **2017**, *18* (7), 2090–2101.

(9) Lodge, Timothy P.; Hiemenz, P. C. *Polymer Chemistry*, 3rd ed.; Taylor & Francis: Boca Raton, Fl, 2020.